ORIGINAL ARTICLE

Journal of Cachexia, Sarcopenia and Muscle 2021; **12**: 476–492
Published online 4 March 2021 in Wiley Online Library (wileyonlinelibrary.com) **DOI:** 10.1002/jcsm.12685

Iron accumulation in skeletal muscles of old mice is associated with impaired regeneration after ischaemia–reperfusion damage

Francesca M. Alves[1,3], Kai Kysenius[2], Marissa K. Caldow[1], Justin P. Hardee[1], Peter J. Crouch[2], Scott Ayton[3], Ashley I. Bush[3], Gordon S. Lynch[1] & René Koopman[1]*

[1]*Centre for Muscle Research, Department of Anatomy and Physiology, The University of Melbourne, Parkville, Victoria, Australia;* [2]*Department of Pharmacology and Therapeutics, The University of Melbourne, Parkville, Victoria, Australia;* [3]*Melbourne Dementia Research Centre, The Florey Institute of Neuroscience and Mental Health, The University of Melbourne, Parkville, Victoria, Australia*

Abstract

Background Oxidative stress is implicated in the insidious loss of muscle mass and strength that occurs with age. However, few studies have investigated the role of iron, which is elevated during ageing, in age-related muscle wasting and blunted repair after injury. We hypothesized that iron accumulation leads to membrane lipid peroxidation, muscle wasting, increased susceptibility to injury, and impaired muscle regeneration.

Methods To examine the role of iron in age-related muscle atrophy, we compared the skeletal muscles of 3-month-old with 22- to 24-month-old 129SvEv FVBM mice. We assessed iron distribution and total elemental iron using laser ablation inductively coupled plasma mass spectrometry and Perls' stain on skeletal muscle cross-sections. In addition, old mice underwent ischaemia–reperfusion (IR) injury (90 min ischaemia), and muscle regeneration was assessed 14 days after injury. Immunoblotting was used to determine lipid peroxidation (4HNE) and iron-related proteins. To determine whether muscle iron content can be altered, old mice were treated with deferiprone (DFP) in the drinking water, and we assessed its effects on muscle regeneration after injury.

Results We observed a significant increase in total elemental iron (+43%, $P < 0.05$) and lipid peroxidation (4HNE: +76%, $P < 0.05$) in tibialis anterior muscles of old mice. Iron was further increased after injury (adult: +81%, old: +135%, $P < 0.05$) and associated with increased lipid peroxidation (+41%, $P < 0.05$). Administration of DFP did not impact iron or measures of lipid peroxidation in skeletal muscle or modulate muscle mass. Increased muscle iron concentration and lipid peroxidation were associated with less efficient regeneration, evident from the smaller fibres in cross-sections of tibialis anterior muscles (−24%, $P < 0.05$) and an increased percentage of fibres with centralized nuclei (+4124%, $P < 0.05$) in muscles of old compared with adult mice. Administration of DFP lowered iron after IR injury (PRE: −32%, $P < 0.05$ and POST: −41%, $P < 0.05$), but did not translate to structural improvements.

Conclusions Muscles from old mice have increased iron levels, which are associated with increased lipid peroxidation, increased susceptibility to IR injury, and impaired muscle regeneration. Our results suggest that iron is involved in effective muscle regeneration, highlighting the importance of iron homeostasis in muscle atrophy and muscle repair.

Keywords Sarcopenia; Muscle mass; Iron; Lipid peroxidation

Received: 19 June 2020; Revised: 8 November 2020; Accepted: 22 January 2021
**Correspondence to: A/Prof. René Koopman, Centre for Muscle Research, Department of Anatomy and Physiology, The University of Melbourne, Parkville, Victoria 3010, Australia. Tel: +61 3 8344 0243, Fax: +61 3 8344 5818, Email: rkoopman@unimelb.edu.au*

Introduction

Ageing is associated with a slow but progressive loss of muscle mass and strength. Although the degree and onset of muscle atrophy varies between individuals, there is a ~1% loss of muscle mass each year that commences midlife[1] and up to 50% total loss by the eighth or ninth decade in severe cases. Depending on the criteria used to define sarcopenia, prevalence in 60- to 70-year-olds is 5–13%, increasing to 11–50% in people older than 80 years.[2] Sarcopenia is linked with an increased risk of hospitalization and mortality and increased healthcare costs.[1] It is often associated with co-morbidities including metabolic diseases (including diabetes and obesity) and neurodegenerative diseases (such as Alzheimer's disease and dementia), with additional impact on the quality of life and health care.[3,4] The incidence of sarcopenia is predicted to increase from 50 million people today to >200 million worldwide over the next 40 years,[5] highlighting the critical need to develop effective interventions.

Accumulation of oxidative stress is implicated in tissue impairment with age.[6] To date, only a few studies have investigated whether iron, an abundant pro-oxidant that elevates in muscle with age, is linked with age-related muscle atrophy.[7,8] These have focused primarily on free Fe^{2+} and its ability to produce reactive oxygen species (ROS) via the Fenton reaction (reviewed in Atamna[9]). Limited information exists regarding the location and modulation of muscle iron, the interaction of iron-containing proteins, and downstream implications beyond Fenton chemistry, such as lipid peroxidation.[10] The study of iron homeostasis in skeletal muscle has been complicated by technical constraints. Studies reporting iron overload in old muscle have employed a variety of methods on homogenates of whole muscle,[7,11–13] but quantification of iron in these preparations cannot distinguish muscle fibres from fibrosis, infiltrating inflammatory cells, adipocytes, fibro/adipogenic progenitors, and muscle stem cells. This is important because macrophages can take up and recycle iron. Thus, an iron overload in muscle may result from increased presence of macrophages rather than iron accumulation in the muscle fibres *per se*.[14] More sophisticated methods are needed to assess iron concentrations in skeletal muscle, the tissue containing approximately 10–15% of total body iron.[15]

Ferritin, the primary storage protein, is often used as a hallmark of iron overload. Iron is found stored either in ferritin or in haem proteins, including haemoglobin, myoglobin, cytochromes, haem thiolates, and non-haem iron and enzyme co-factors.[16] Iron is essential for cell respiration and other enzymatic processes that are abundant in highly metabolic tissue such as skeletal muscle, and so investigations of iron overload must consider multiple iron-containing proteins because their implications could differ. Regardless of the precise location of iron, excess iron in skeletal muscle may also impact the susceptibility of this tissue to injury and its ability to regenerate. For example, mice with iron overload (via intraperitoneal injection) had decreased expression of satellite cell markers and delayed muscle regeneration after injury, as evident from the decrease in the size of regenerating myofibres, reduced expression of myoblast differentiation markers, and signalling pathways involved in cell growth (MAPK).[13] Furthermore, iron overload suppressed the differentiation of C2C12 myoblasts. Because a role for iron in injury and repair has only been investigated through systemic administration of iron,[13] a more detailed investigation on the critical role of iron in the regulation of skeletal muscle mass, metabolism, and repair is needed, particularly in a clinically relevant model of muscle injury in old mice.

As an accumulation of iron in tissues is associated with increased oxidative stress,[17] we hypothesized that iron accumulation in muscles of old mice would increase membrane lipid peroxidation leading to muscle wasting, increased susceptibility to injury, and impaired muscle regeneration. The aims were to determine (i) the changes in iron homeostasis in skeletal muscle during ageing and (2) whether treatment with an iron chelator (DFP) could redistribute iron from muscle with beneficial effects on skeletal muscle mass and recovery after injury.

Methods

Animals

All experiments were approved by the Animal Ethics Committee of The University of Melbourne and conducted in accordance with the Australian Code of Practice for the Care and Use of Animals for Scientific Purposes as stipulated by the National Health and Medical Research Council (Australia). Male and female mice were used for all experiments. During the intervention, all mice were housed under a 12:12 h light–dark cycle with temperature control in the Biological Research Facility (The University of Melbourne) and monitored weekly. Wild-type 129SvEv FVBM (3- and 22- to 24-month-old) mice were sourced from Taconic Biosciences (Rensselaer, NY, USA). C57BL/6 mice (4 months old) were sourced from Animal Resources Centre (Canning Vale, WA, Australia).

Experimental outline

Deferiprone administration

Deferiprone (3-hydroxy-1,2-dimethyl-4(1*H*)-pyridine; Sigma-Aldrich, Castle Hill, NSW, Australia) was dissolved in the drinking water. For long-term (12 week) DFP treatment, 129SvEv FVBM mice were treated with 100 mg/kg DFP (Ayton *et al*.[18]). For short-term DFP treatment, mice were assigned to be treated with (i) 150 mg/kg DFP for 1 week prior to

DOI: 10.1002/jcsm.12685

ischaemia–reperfusion injury (IRI) or (ii) 150 mg/kg DFP for 2 weeks after IRI. Long-term (12 week) DFP treatment was conducted in old 129SvEv FVBM mice (starting at 19 months).

Ischaemia–reperfusion injury

The IRI model has clinical relevance to the ageing population as some surgeries in older patients (including joint replacements and limb revascularization) require temporary occlusion of blood flow, which induces ischaemia and compromises the muscle's local milieu. In addition, it is also well established that limb ischaemia and reperfusion can result in severe damage via the generation of ROS.[19–21] The initial ischaemia–reperfusion (IR) time course was conducted in C57BL/6 mice (4 months old). Mice were anaesthetized via intraperitoneal injection (100 mg/kg ketamine and 10 mg/kg xylazine, Clifford Hallam Healthcare, Eastern Creek, NSW, Australia) with further maintenance of anaesthesia via oxygen–isoflurane (Isoflurane SomnoSuite, Kent Scientific, Torrington, CT, USA) in an anaesthetic chamber, 2–3% at 0.5 L/min. Once anaesthetized and non-responsive to tactile stimuli (tail/toe pinch), orthodontic rubber bands (Dentaurum Australia, Mortlake, NSW, Australia) were positioned high on the right hindlimb (Crawford *et al.*[22]). The occlusion of blood vessels and reduction in blood flow were assessed via laser Doppler imaging (Moor Instruments, Axminster, UK) before, during, and after ischaemia (immediately after reperfusion commenced). After 90 min of ischaemia, the bands were removed using small scissors, blood flow restored to the hindlimb, and animals recovered on a heat pad until fully conscious. Mice were killed via cervical dislocation at 4 h, 1 day, 3 days, 7 days, and 14 days after IR injury, and selected tissues were collected and stored at −80°C for later analysis.

For age comparison experiments, 3-month-old (adult) and 22- to 24-month-old 129SvEv FVBM mice (old) were used. IRI was performed as described earlier. Endpoint measurements and samples were collected 14 days after IRI. Mice were killed as stated earlier.

Whole-body functional assessments

Grip strength

Forelimb strength was assessed using a grip strength metre (Columbus Instruments, Columbus, OH, USA).[23] Briefly, mice grasped a triangular metal ring connected to a force transducer while the tail was held and pulled gently until the grip was broken. Peak force was measured in kilograms. Each mouse performed the test five times within 2 min, with adequate rest time (30 s) between attempts.

Body composition

Before and after recovery from IRI, whole-body composition was analysed using magnetic resonance relaxation analysis of live body composition of fat tissue, lean tissue, free water, and total water (LF50, Bruker, Billerica, MA, USA).

Metabolic measurements

Mice were housed individually for 1.5 days in airtight calorimetry chambers connected to a multiplexed gas sensor unit to assess VO_2 and VCO_2 (Promethion; Sable Systems International, North Las Vegas, NV, USA). The respiratory exchange ratio was calculated as VCO_2/VO_2. Energy expenditure was calculated from VO_2 and respiratory exchange ratio using Weir constants and normalized to lean mass.[24] Food and water intake were recorded every 15 min. Physical activity was recorded via beam breaks (BXYZ Beambreak Activity Monitor; Sable Systems International), and mice had access to a running wheel.

Endpoint measurements

Tissue collection

At the end of the treatment period, mice were anaesthetized with 0.2 mL of sodium pentobarbitone (Nembutal; 60 mg/kg; Sigma-Aldrich, intraperitoneal injection) and killed via cervical dislocation followed by cardiac excision. Skeletal muscles of the hindlimb [tibialis anterior (TA), gastrocnemius, extensor digitorum longus, and soleus], heart, kidney, spleen, and liver were excised, weighed, snap frozen in liquid nitrogen, and stored at −80°C for later analysis. Half of the TA muscles were mounted in optimal cutting temperature embedding compound (Tissue-Tek, Sakura Finetek, Torrance, CA, USA), frozen in liquid nitrogen-cooled isopentane, and stored at −80°C for later analysis. The tibia bone was dissected, and length was measured using digital callipers.

Blood serum collection

Blood was collected from the intact heart. Whole blood droplets were used to measure resting blood glucose using a blood glucose meter (Accu-Chek, North Ryde, NSW, Australia) and resting haematocrit levels (HemoCue® Hb 201+ System, Mt Waverley, VIC, Australia).

Biochemical analysis

Protein extraction and immunoblotting

Tibialis anterior muscles (10–30 mg) were homogenized in ice-cold buffer (TBS; 50 mM Tris–Cl, pH 7.6; 150 mM NaCl; Sigma-Aldrich; in Milli-Q H_2O) containing 2% (v/v) cOmplete™ EDTA-free protease inhibitor (Roche, Hawthorn, VIC, Australia) in tubes containing a 1.0 mm zirconia/silica beads (Daintree Scientific, St Helens, TAS, Australia) using a cooled Precellys 24® tissue homogenizer (1 cycle of 20 s at 5500 r.p.m.; Sapphire Bioscience, Redfern, NSW, Australia). After brief centrifugation, whole homogenates were transferred to a new set of tubes and then rotated at 4°C for 10 min. Lysates were centrifuged for 15 min at 15 000 *g*., and the supernatant

was collected. Total protein concentration of the supernatant was determined using the Bio-Rad DC protein assay kit per the manufacturer's instructions (Bio-Rad Laboratories, Gladesville, NSW, Australia).

Homogenates (0.5–1 μg/μL) were denatured at 95°C in 4× Laemmli sample buffer containing dithiothreitol (Sigma-Aldrich) for 5 min. Protein (5–10 μg) was separated by 4–20% SDS-PAGE (Criterion TGX Stain-Free Precast Gels; Bio-Rad Laboratories) for 1.5 h at 150 V. Proteins were transferred onto 0.2 μM nitrocellulose membranes using the Transblot Turbo system (Bio-Rad Laboratories), with a constant output of 25 V for 7 min. Proteins were visualized prior to and following transfer using the ChemiDoc™ MP Imaging System (Bio-Rad Laboratories). Membranes were blocked using 5% BSA in TBST at room temperature for 2 h and then incubated in primary antibodies in 5% BSA in TBST overnight at 4°C [4HNE, ALAS-1, cytochrome *c*, FTH, PGC-1a, COX IV, myoglobin (Abcam, Cambridge, UK), ACSL4 (Santa Cruz Biotechnology, Santa Cruz, CA, USA), and TFR1 (Alpha Diagnostic, San Antonio, TX, USA)]. Membranes were washed five times with TBST (5 min each) prior to incubation with an appropriate horseradish peroxidase-conjugated secondary antibody. Membranes were washed five times with TBST, and proteins were visualized with SuperSignal® West Femto Maximum Sensitivity Substrate (Thermo Fisher Scientific, Scoresby, VIC, Australia) using the ChemiDoc™ MP Imaging system (Bio-Rad Laboratories). The density of bands was quantified using Image Lab software (Bio-Rad Laboratories) and normalized to total protein. Images of stain-free gels were used to quantify total protein loading for each lane.

Citrate synthase enzyme activity

Gastrocnemius muscles were homogenized using a cooled Precellys 24 tissue homogenizer (1 cycle of 20 s at 5500 r.p.m.; Sapphire Bioscience) in homogenizing buffer [10 mM Tris HCl (pH 7.4), 100 mM NaCl, 1 mM EGTA, 1 mM EDTA, 1% Triton X-100, 10% glycerol, 0.1% SDS, 20 mM $Na_4P_2O_7$, 2 mM Na_3VO_4, 1 mM NaF, 0.5% sodium deoxycholate, and 1 mM PMSF]. The homogenates were frozen under liquid nitrogen and thawed four times to disrupt the mitochondria to expose citrate synthase. Total muscle protein was determined in triplicate by the method of Bradford, and the protein concentration of all samples was equalized. Citrate synthase activity was determined, normalized to total protein content, and expressed in nanomole per milligram protein per minute, as described previously.[25,26]

RNA extraction and quantitative PCR

Total RNA was extracted from 10–20 mg of TA muscle using a commercially available kit, according to the manufacturer's instructions (RNeasy Mini Kit, Qiagen, Chadstone, VIC, Australia). RNA quality and concentration were determined using the Nanodrop 1000 (Thermo Fisher Scientific). First-strand cDNA was generated using the iScript™ Reverse Transcription Supermix according to manufacturer's instructions (Bio-Rad Laboratories). Quantitative PCR was performed in duplicate using the Bio-Rad CFX384 PCR system (Bio-Rad Laboratories) with reaction volumes of 10 μL, containing SsoAdvanced™ Universal SYBR® Green Supermix (Bio-Rad Laboratories), forward and reverse primers, and cDNA template (2 ng/μL). Data were analysed using a comparative quantification cycle (Cq) method where the amount of target was normalized to cDNA content (ng/mL × 10–12). CDNA content was determined using Quant-iT™ OliGreen™ ssDNA Assay Kit, as per the manufacturer's instructions. Primers were designed using NCBI primer Basic Local Alignment Search Tool (BLAST), and specificity was confirmed using BLAST. A melting point dissociation curve was generated by the PCR instrument for all PCR products to confirm the presence of a single amplified product. Primer sequences are listed in *Table* 1 or described elsewhere.[23,27–29]

Histology

Serial sections (10 and 30 μm) were cut transversely through the TA muscle using a refrigerated (−2°C) cryostat (CTI Cryostat; IEC, Needham Heights, MA, USA). Sections were stained with haematoxylin and eosin (H&E) to determine general muscle architecture[30]; CD68/F480 for determination of macrophage infiltration[31]; modified Perls' stain for iron deposition[32]; and Van Gieson's stain for collagen deposition.[23]

Digital images of H&E and CD68/F480/DAPI in *Figures* 1 and 2 and Supporting Information, *Figure* S1 were obtained using an upright microscope with camera (Axio Imager D1; Carl Zeiss, Wrek, Göttingen, Germany), controlled by AxioVision AC software (AxioVision AC Rel. 4.8.2; Carl Zeiss Imaging Solutions, Wrek, Göttingen, Germany). Images were quantified with AxioVision 4.8.2 software. Digitally captured images (×120 magnification) with a minimum of three fields of view per muscle cross-section were processed and analysed.

For all other imaging, slides were submitted for digitalization at the Australian Phenomics Network Histopathology and Organ Pathology slide scanning service (Melbourne, VIC, Australia; manufacturer: 3DHISTEC; model: PANNORAMIC SCAN II; objective: Carl Zeiss Plan-Apochromat 20×/NA 0.8, using a Point Grey Grasshopper 3CCD monochrome camera with LED-based RGB illumination unit). Scans were viewed, and images were taken using CaseViewer software. Subsequent analysis was performed using Fiji software.[33]

Table 1 Primer sequences for RNA extraction and quantitative PCR of tibialis anterior muscles

Gene name	GenBank accession no.	Forward sequence (5′–3′)	Reverse sequence (5′–3′)	Amplicon length
Alas-1	NM_001291835.1	CATTCGACATTTGACAGGCGG	GCCAGACAACGCAAAGAGTC	120
Cpt-1	NM_009948	GTCGCTTCTTCAAGGTCTGG	AAGAAAGCAGCACGTTCGAT	232
Cox IV	NM_009941	ACTACCCCTTGCCTGATGTG	GCCCACAACTGTCTTCCATT	188
F4/80	NM_010130.4	CATCAGCCATGTGGGTACAG	CATCACTGCCTCCACTAGCA	251
CD163	NM_001170395.1	CCTCTGCTGTCACTAACGCT	TTCATTCATGCTCCAGCCGT	143
CD80	NM_001359898.1	ACAACAGCCTTACCTTCGGG	TTTGCAGAGCCAGGGTAGTG	179

Laser ablation inductively coupled plasma mass spectrometry

Laser ablation inductively coupled plasma mass spectrometry (LA-ICP-MS) experiments were carried out as described previously for tissue imaging[34,35] and μ-droplet analysis.[36] A NewWave Research NWR213 laser ablation system (Kenelec Scientific, Mitcham, VIC, Australia) with a standard 2 V cell was used for all analyses. Argon was used as the carrier gas (1.2 L/min). All measurements were performed using an Agilent 8800 triple quadrupole ICP-(QQQ)-MS system with 'cs' lenses. The ICP-QQQ-MS system used was previously optimized to 'no gas' tuning parameters to maximize ion focusing and transmission via the Q2 ion-guide and collision/reaction cell.[37]

For tissue imaging, silica glass microscope slides (Menzel-Gläser Superfrost® Plus; Thermo Fisher Scientific) with 30-μm-thick muscle sections were placed in a 10 × 10 cm ablation cell together with matrix-matched elemental standards for quantitative analysis. Muscle sections were ablated with a 60 μm square beam laser using a series of rasters and a scanning speed of 240 μm/s and elemental data collected for carbon (^{13}C), phosphorus (^{31}P), and iron (^{56}Fe). For high-resolution images for Perls' stain matching, selected sections were ablated with a 15 μm square beam laser using a series of rasters and a scanning speed of 30 μm/s.

For μ-droplet analysis,[35,36] up to 150 droplets (0.5 μL) of samples and standards were deposited onto microscope slides manually in triplicates. Standards and samples were deposited in rows within the 5 × 2.5 cm working area of a single slide and then air dried in a particle-free environment overnight. A square beam 100 μm wide scanned at 200 μm/s and 0.3–0.5 J/cm^2 fluence laser power was used to remove all deposited material while not ablating the supporting glass (minimum fluence threshold for ablation of silicate glass 2.4 J/cm^{238}), resulting in a total analysis time of approximately 8–14 h per slide. The ICP-QQQ-MS system was configured to measure the mass-to-charge (*m*/*z*) ratios for elements carbon (^{13}C), phosphorus (^{31}P), magnesium (^{24}Mg), calcium (^{44}C), and iron (^{56}Fe).

Single-line scans from LA-ICP-MS analysis (as.csv files) were collated into hyperspectral images using iolite (v.3; The University of Melbourne, Parkville, VIC, Australia) with the Biolite add-on for image analysis[30] (*Figure* 1E; see Hare *et al.*[35] for a visual tutorial). Modifications to the image analysis code were made using Igor Pro (v7; WaveMetrics, Inc., Portland, OR, USA). Region of interest tool was used to extract mean ($\bar{x}$) counts per second for each *m*/*z* from the desired area. For μ-droplet analysis, external calibration was performed via linear regression analysis using a 4-point (including matrix blank) calibration curve in Prism (v7, GraphPad Software Inc., La Jolla, CA, USA). All μ-droplet dilution series were analysed in triplicate or as otherwise stated.

Statistical analysis

Data were analysed with GraphPad Prism software Version 7 (GraphPad Software Inc.). Unpaired *t*-tests were used for comparisons between two groups. For comparisons between more than two groups, a one-way or two-way analysis of variance was used, as appropriate, with Tukey's *post hoc* multiple comparisons test when significance was detected. The level of significance was set at $P < 0.05$ for all comparisons. All values are presented as mean ± standard error of the mean.

Results

Old 129SvEv FVBM mice exhibit sarcopenia

Old 129SvEv FVBM mice (22–24 months; $n = 12$) showed structural and functional muscle impairments compared with younger adult FVBM mice (3 months; $n = 12$). Old mice had a significantly higher body mass (+53%, $P < 0.05$; *Figure* 1A) and altered body composition compared with adult mice; more body fat (+207%, $P < 0.05$; *Figure* 1B) and free water (+28%, $P < 0.05$; *Figure* 1B); and reduced lean tissue mass (−29%, $P < 0.05$; *Figure* 1B). Hindlimb muscle masses were lower relative to body mass, including the TA (−41%, $P < 0.05$; *Figure* 1C), gastrocnemius (GAST: −33%, $P < 0.05$; *Figure* 1C), and extensor digitorum longus (EDL: −45%. $P < 0.05$, *Figure* 1C). In addition to old mice having smaller muscles, individual muscle fibre diameter (in TA muscles, *Figure* 1E) was reduced (−14%, $P < 0.05$; *Figure* 1F) with signs of regeneration, demonstrated by the increased number of fibres with centralized nuclei (+2275 %, $P < 0.05$;

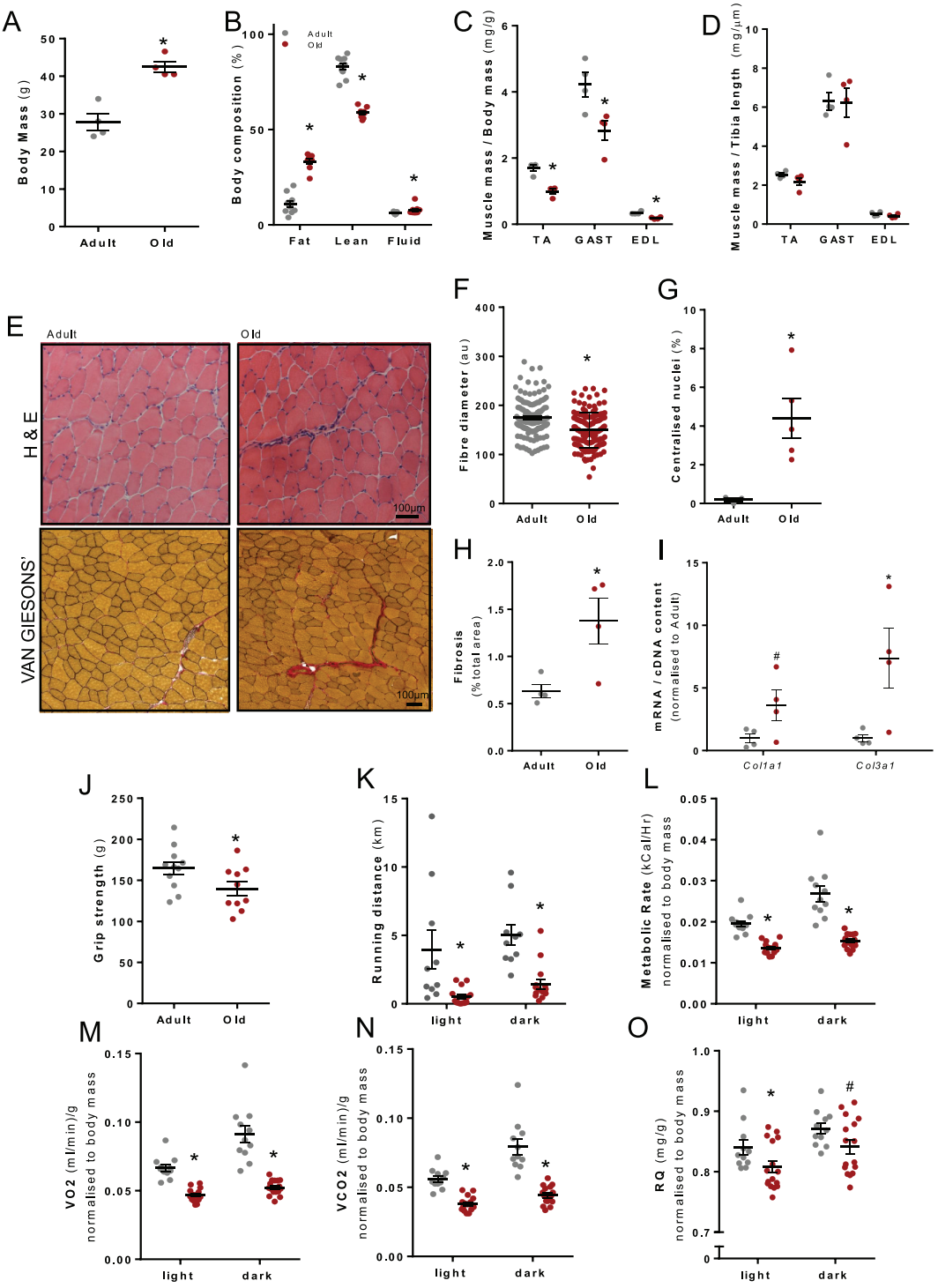

Figure 1 Old mice (22–24 months, $n = 12$) showed structural and functional muscle decline compared with adult mice (12 weeks, $n = 12$). (A) Old mice had a significantly higher body mass and (B) more body fat and free water and lower overall lean body mass. (C) Old mice had smaller hindlimb muscles relative to body mass, tibialis anterior (TA), gastrocnemius (GAST), and extensor digitorum longus (EDL), (D) but unchanged when normalized to tibia length. (E) Haematoxylin and eosin-stained and Van Gieson-stained TA muscle cross-sections revealed (F) reduced fibre diameter, (G) a higher percentage of centralized myonuclei, (H) increased fibrosis, and (I) Col1a1 and Col3a1 mRNA normalized to cDNA content. Old mice showed functional decline evident from (J) reduced raw grip strength and (K) reduced maximum running distance over a 24 h period. When mice were placed in metabolic cages for a 24 h period (6 a.m. to 6 p.m. light and 6 p.m. to 6 a.m. dark), analysis of metabolic parameters revealed age-related reductions in (L) metabolic rate (kcal/h), (M) VO_2 (mL/min), (N) VCO_2 (mL/min), and (O) respiratory quotient (RQ). Data presented as mean ± standard error of the mean. Data were analysed using Student's *t*-test (A–G) and two-way analysis of variance with Sidak's *post hoc* test (I–L). $^{*}P \leq 0.05$ and $^{\#}P \leq 0.1$.

DOI: 10.1002/jcsm.12685

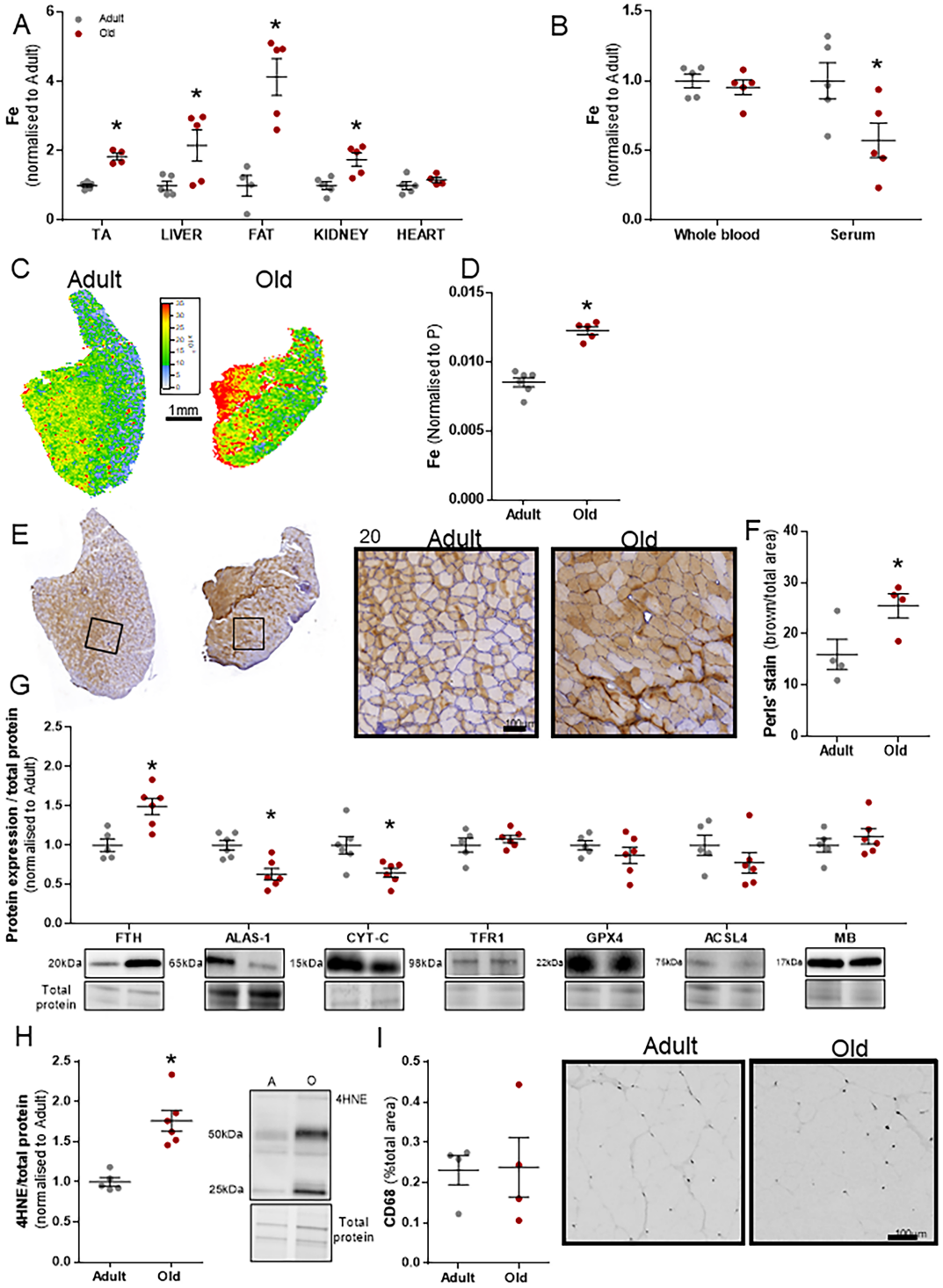

Figure 2 Old mice (22–24 months, *n* = 6) show iron (Fe) dysregulation across multiple organs compared with adult mice (12 weeks, *n* = 6). Analysis of several key organs showed consistent iron elevation in old mice (A). Iron levels were unchanged in whole blood but significantly lower in serum of old mice (B). Total elemental iron elevation in tibialis anterior (TA) was present in laser ablation inductively coupled plasma mass spectrometry images highlighting all oxidative states of Fe normalized to phosphorus (P) (C, D) and modified Perls' stain (brown = ferric Fe^{3+} deposits) (E, F). Western blots of homogenized TA muscles showed significant increases in ferritin (FTH), decreases in 5′-aminolevulinate synthase 1 (ALAS-1) and cytochrome *c* (CYT-C), and no change in transferrin receptor 1 (TFR 1), glutathione peroxidase-4, (GPX-4), acyl-CoA synthetase long-chain family member 4 (ACSL4), and myoglobin (MB) (G). Lipid peroxidation was determined using an antibody against 4HNE (H) and inflammation by CD68 area as a percentage of total muscle area (I). Data presented as mean ± standard error of the mean. Data were analysed using Student's *t*-test. *$P \leq 0.05$.

DOI: 10.1002/jcsm.12685

Figure 1G) and increased deposition of fibrosis (TA: +117%, $P < 0.05$, *Figure* 1H) associated with increased *Col1a1* and *Col3a1* mRNA expression (*Figure* 1I).

In old mice, forelimb strength and whole-body function were reduced, as evidenced by reduced grip strength (−15%, $P < 0.05$; *Figure* 1J) and running distance over a 24 h period (light: −87% and dark: −71%, $P < 0.05$; *Figure* 1K). Metabolic assessments in old mice over a 24 h period (6 a.m. to 6 p.m. *light* and 6 p.m. to 6 a.m. *dark*) using Promethion metabolic cages revealed reductions in energy expenditure (light: −30% and dark: −43%, $P < 0.05$; *Figure* 1L), oxygen consumption (VO_2 in mL/min; light: −29% and dark: −43%, $P < 0.05$; *Figure* 1M), carbon dioxide production (VCO_2 in mL/min; light: −32 and dark: −44%, $P < 0.05$; *Figure* 1N), and respiratory quotient (light: −4% and dark: −3.5%, $P < 0.1$; *Figure* 1O).

Muscles from old mice have increased intracellular iron and lipid peroxidation

Iron dysregulation was present systemically in old mice. Multiple tissues from old mice exhibited increased iron levels in tissue homogenate from multiple organs: liver (+116%, $P < 0.05$), fat (+313%, $P < 0.05$), and kidney (+75%, $P < 0.05$) (*Figure* 2A). Total elemental iron concentration was lower in the serum of old compared with adult mice ($P < 0.05$; *Figure* 2B). To determine spatial distribution of iron, iron was measured via LA-ICP-MS in the TA muscle, which showed significantly higher iron abundance in old mice (+43%, $P < 0.05$; *Figure* 2C and 2D). Similarly, when iron was assessed via modified Perls' stain that measures only ferric iron (Fe^{3+}), we observed a significant increase (+60%, $P < 0.05$; *Figure* 1E and 1F) in muscles of old mice.

Importantly, iron was observed to be increased in muscle, and infiltration of macrophages could not account for the bulk iron changes. While the iron storage protein ferritin (FTH) was increased (+50%, $P < 0.05$; *Figure* 2G), the rate-limiting enzyme for haem synthesis, ALAS-1, was decreased (−36%, $P < 0.05$) along with CYT-C, a haem-containing mitochondrial protein important for respiration (−35%, $P < 0.05$) (*Figure* 2G). No changes were observed in mRNA (*Figure* S1A) and protein expression (*Figure* S1B) of other selected mitochondrial markers and citrate synthase activity (*Figure* 1C). Iron is well known to generate oxidative stress via the Fenton reaction. To determine whether the iron overload in skeletal muscle was associated with increased lipid peroxidation, we performed immunoblot analysis of 4HNE, a validated marker for lipid peroxidation. Muscles of old mice showed a concomitant increase of iron and lipid peroxidation (+76%, $P < 0.05$; *Figure* 2H). GPX4 is the checkpoint for membrane phospholipid peroxidation, and this was not significantly decreased in the muscle of old mice. ACSL4 is a protein required for the esterification of polyunsaturated fatty acids, which is a necessary requirement for iron-induced peroxidation of lipids, but this protein was not changed in muscle either. Although we observed an increase in *Cd68* (+513, $P < 0.05$), *Cd206* (+275, $P < 0.1$), *Cd80* (+395, $P < 0.1$), and *Ccl2* (+447, $P < 0.05$) mRNA expression in old mice (*Figure* S1D), iron overload was not associated with an increased infiltration of inflammatory cells (*Table* 2), and the amount of CD68-positive cells in muscle cross-sections from adult and old mice was not different (*Figure* 2I). Total iron was positively correlated (Pearson's *r*) with FTH (*r*: 0.687 and $P = 0.0006$), lipid peroxidation (4HNE; *r*: 0.9300 and $P < 0.0001$), and fibrosis (*r*: 0.7181 and $P = 0.0001$) (*Table* 2).

Chronic deferiprone treatment counteracts iron overload in the liver but not muscle in old mice

We tested the hypothesis that iron chelation would reduce skeletal muscle iron concentration and subsequently attenuate lipid peroxidation. We treated old mice with a commonly used iron chelator DFP (100 mg/kg/day) for 12 weeks (*Figure* 3A). DFP treatment did not affect resting blood glucose (*Figure* 3B) or blood haematocrit (*Figure* 3C). DFP treatment did not result in changes in TA muscle mass (*Figure* 3D), body composition (*Figure* 3E), maximum grip strength (*Figure* 3F), or running distance (*Figure* 3G). In addition, chronic DFP treatment did not lower iron in two different muscles with varying fibre type distributions, that is, the TA (predominantly fast) and SOL (predominantly slow) muscles (*Figure* 3H). Similarly, iron-related proteins (FTH and MB) and lipid peroxidation (4HNE) were not different between groups (*Figure* 3I).

To determine the effect of systemic DFP treatment, multiple organs were subsequently assessed for changes in iron. DFP lowered iron only in the liver (−55%, $P < 0.05$;

Table 2 Correlation analyses in muscles from young and old mice

Fe vs.	*r*	*P*
FTH	0.6873	0.0006****
4HNE	0.9300	<0.0001****
Fibrosis	0.7181	0.0001***
CYT-C	−0.7080	0.0003***
CS	−0.2241	0.3041, ns
CD68	0.3543	0.1152, ns
Modified Perls'	0.9569	<0.0001****

Uninjured and injured hindlimbs of adult and old mice were pooled together ($n = 24$). Total iron (Fe measured by laser ablation inductively coupled plasma mass spectrometry) was positively correlated (Pearson's *r*) with iron storage protein ferritin (FTH), lipid peroxidation (4HNE), fibrosis (Van Gieson's), haem protein cytochrome *c* (CYT-C), and ferric iron determined by modified Perls' stain. No correlation was found in a marker of mitochondria content, citrate synthase activity (CS), and immunohistochemistry of inflammatory mediator cluster of differentiation 68 (CD68). CS was measured in the gastrocnemius muscles. All other measurements were taken from the tibialis anterior muscles.

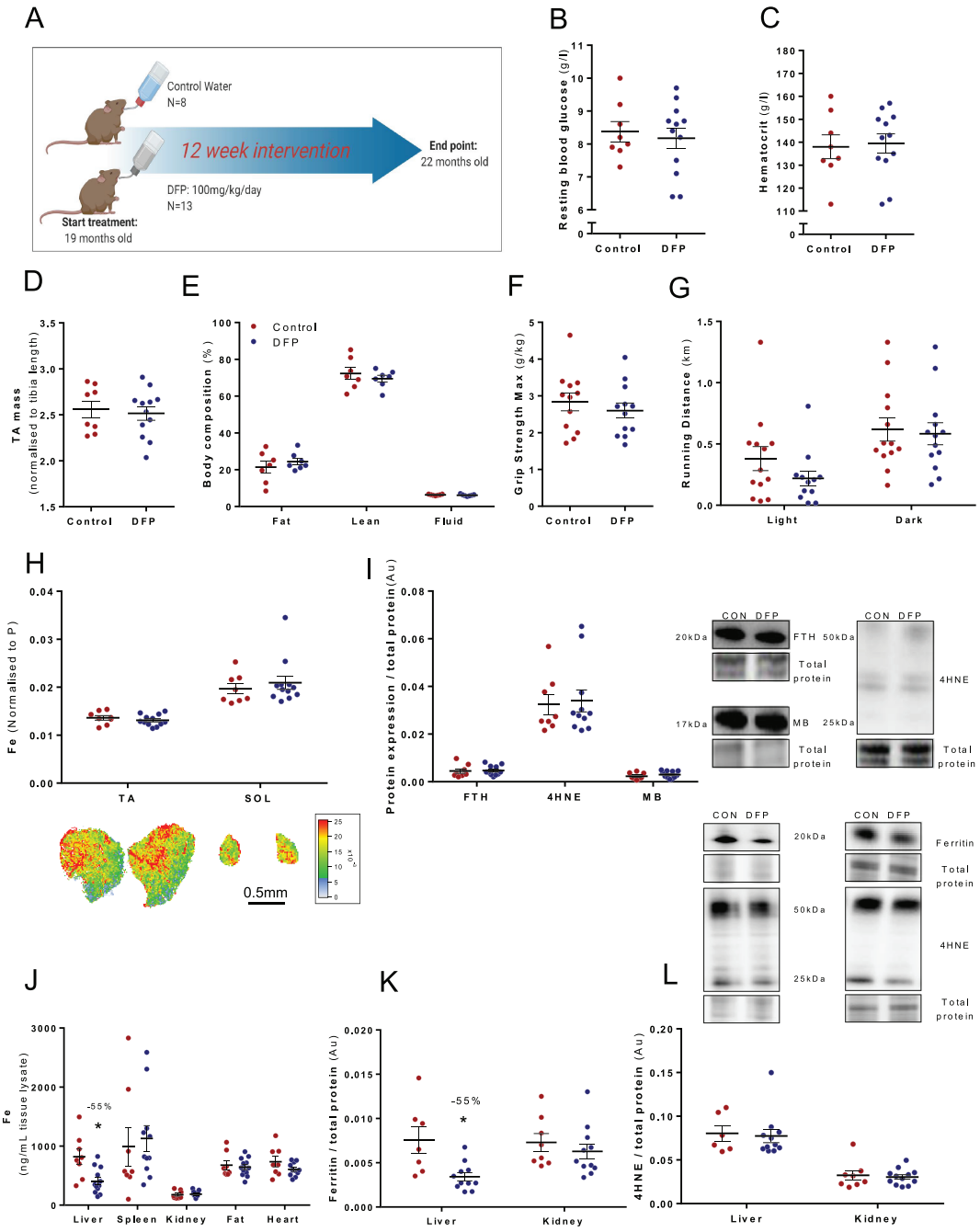

Figure 3 Old mice (18 months) were treated with deferiprone (DFP: 100 mg/kg/day; *n* = 13) or control administered via drinking water (*n* = 8) for 12 weeks (A). There was no change in resting blood glucose (B) and haematocrit (C) levels from whole blood or tibialis anterior muscle mass (TA) (D) and body composition (E). Functional analysis performed during Week 12 also showed no change in maximum grip strength (F) or running distance (G). Iron levels were analysed via laser ablation inductively coupled plasma mass spectrometry in two muscles with different muscle fibre type distributions, TA (predominantly fast) and soleus (SOL; predominantly slow), but no changes were evident (H). Key iron-related proteins in the TA muscle were also unchanged (I). Iron levels for the liver, spleen, kidney, fat, and heart were analysed via laser ablation inductively coupled plasma mass spectrometry, but only the liver showed a significant reduction with treatment (J). Western blots showed that ferritin was reduced in the liver but not kidney (K); however, lipid peroxidation (4HNE) was unchanged in both liver and kidney (L). Data presented as mean ± standard error of the mean. Data were analysed using Student's *t*-test. $^*P \leq 0.05$.

Figure 3J). Ferritin protein expression but not lipid peroxidation was decreased in the liver (−55%, $P < 0.05$; *Figure* 3K and 3L).

Iron is increased during the later stages of muscle repair after ischaemia–reperfusion injury in adult C57BL/6 mice

We conducted a time course study to assess the biochemical events and severity of insult after IRI. Early time points showed an increase in TA mass (4 h: +24%, $P < 0.05$ and 1 day: +24%, $P < 0.05$; *Figure* S2B), which coincided with an increase in $[Ca^{2+}]$ (4 h: +660%, $P < 0.05$ and 1 day: +645%, $P < 0.05$; *Figure* S2E), indicative of increased oedema and swelling after ischaemia. By Day 7, TA mass showed a trend to decrease (−11%, $P < 0.1$; *Figure* S2B), but muscle mass was restored by Day 14. Infiltration of inflammatory cells occurred after oedema and swelling at Day 3 (CD68: +178%, $P < 0.05$ and F480: +567%, $P < 0.05$) and Day 7 (CD68: +1520%, $P < 0.05$ and F480: +3286%, $P < 0.05$) (*Figure* S2C and S2F). Iron concentrations were increased at Day 7 (+75%, $P < 0.05$) and remained elevated at Day 14 (70%, $P < 0.05$) (*Figure* S2D), when regenerated fibres have prominent centralized nuclei (*Figure* S2A). Fibrosis elevation preceded and overlapped with both inflammation and iron occurring at Day 1 (+530%, $P < 0.05$) to Day 14 (+1358%, $P < 0.05$, *Figure* 2G).

Elevated iron in muscles of old mice is associated with impaired or delayed regeneration after ischaemia–reperfusion injury

Based on our time course experiments in young C57BL/6 mice, we assessed changes in iron at Day 14 after IR injury in adult and old 129SvEv FVBM mice. Iron concentration was increased 14 days after injury in adult 129SvEv FVBM mice (+81%, $P < 0.05$) but increased to a greater extent in old mice despite the higher basal iron (+135%, $P < 0.05$; *Figure* 4A). The iron elevation in muscles of old mice was associated with an increased elevation in lipid peroxidation (4HNE: +41%, $P < 0.05$; *Figure* 4B), increased ferritin (adult: +75%, $P < 0.05$ and old: +131%, $P < 0.05$; *Figure* 4C), and increased fibrosis (adult: +579%, $P < 0.05$ and old: +527%, $P < 0.05$; *Figures* 4G and S3A). The mRNA expression of collagen mediators Col1a1 and Col3a1 was significantly increased after injury in the muscles of old mice (Col1a1: +4264%, $P < 0.1$ and Col3a1: +3254%, $P < 0.05$; *Figure* S3B). Injured muscles in adult and old mice had increased myoglobin (adult: +153%, $P < 0.05$ and old: +143%, $P < 0.05$; *Figure* 4D). Cytochrome *c* protein expression (*Figure* 4E) and citrate synthase activity (*Figure* 4F) were not significantly affected by IR injury but were significantly reduced in the muscles of old mice.

The increased muscle iron concentration and lipid peroxidation were associated with less efficient regeneration, evident from the smaller fibres in cross-sections of TA muscles (−24%, $P < 0.05$; *Figure* 4H) and an increased percentage of fibres with centralized nuclei (+4124%, $P < 0.05$; *Figure* 4I) in muscles of old compared with adult mice.

The total amount of elemental iron (LA-ICP-MS; *Figure* 4K) corresponded to increased ferric iron, as shown in representative images with the modified Perls' stain where iron accumulation occurred within muscle fibres (adult: +57%, $P < 0.05$ and old: +110%, $P < 0.05$; *Figure* 4O and 4P). Inflammation, assessed as CD68 infiltration (*Figure* 4L and 4M) and mRNA expression (*Figure* S3C) and the percentage of non-muscle tissue (*Figure* 4N), was not different between groups but highly variable.

Deferiprone treatment before or after ischaemia–reperfusion injury does not improve muscle regeneration in old mice

Treatment with DFP 7 days before IR injury (150 mg/kg/day) or during recovery (14 days DFP: 150 mg/kg/day) reduced total elemental iron (PRE: −32%, $P < 0.05$ and POST: −41%, $P < 0.05$; *Figure* 5A and 5I) and ferric iron (POST: −31%, $P < 0.05$; *Figure* 5B and 5J). Despite the reduction in skeletal muscle iron, there was no change in fibre diameter (*Figure* 5C), level of inflammatory cell infiltration (*Figure* 5D and 5E), or percentage of fibres with centralized nuclei (*Figure* 5F). Haematoxylin and eosin staining of muscle cross-sections showed increased non-muscle tissue (adipocytes) within muscles treated with DFP (PRE: +155%, $P < 0.05$ and POST: +127%, $P < 0.05$; *Figure* 5G and 5H), indicating that chelating iron within the setting of injury repair may be detrimental to muscle regeneration. The Van Gieson's staining revealed that the non-muscle tissue was not associated with fibrosis as fibrotic infiltration was not different between groups (*Figure* S4A and S4B). Iron was negatively correlated with non-muscle tissue (*Table* 3). Citrate synthase activity was significantly reduced by DFP-PRE treatment (−27%, $P < 0.05$, *Figure* S4E), whereas protein expression of PGC-1a and COX IV was not altered significantly. We did not observe overt changes in mRNA expression of inflammatory markers following DFP treatment (*Figure* S4D and S4F).

Discussion

Excessive oxidative stress is a well-known contributor to muscle atrophy as observed in mammalian ageing.[6] To date, few

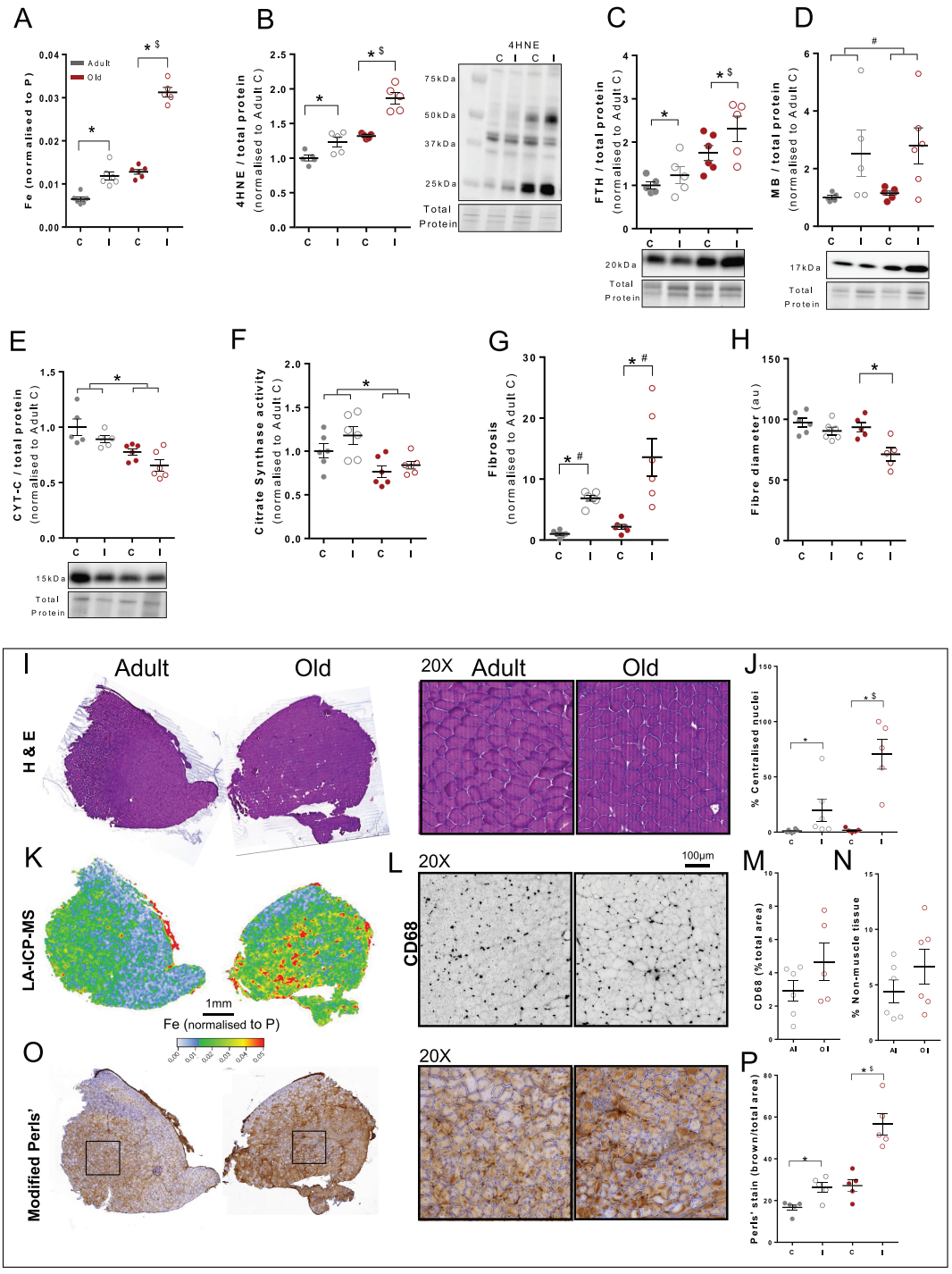

Figure 4 Adult and old mice (n = 6 per group) were subject to ischaemia–reperfusion injury (IRI) and 14 days of recovery. This involved application of an orthodontic rubber band above the knee to the right leg (I = injured) for a 90 min period of ischaemia and subsequent reperfusion. Injured legs were compared with contralateral left uninjured legs (C = control). Grey = adult and red = old. Total elemental iron elevation in tibialis anterior (TA) muscles was increased (A) along with lipid peroxidation (4HNE) (B) and ferritin (FTH) (C). Myoglobin (MB) was increased in both injured legs (D), and cytochrome *c* (CYT-C) (E) and citrate synthase activity were decreased with age (F). Injured legs from old mice had increased fibrosis (Van Gieson's) (G) and a smaller fibre diameter (H) determined from haematoxylin and eosin-stained sections of TA muscles (I) and an increased percentage of centralized nuclei (J). The total amount of elemental iron (laser ablation inductively coupled plasma mass spectrometry; K) corresponded to increased ferric iron, as shown in representative images of the modified Perls' stain (O) (brown = ferric Fe^{3+} deposits) and quantified (P). Inflammation based on F4/80 and CD68 infiltration (L, M) and percentage of non-muscle tissue (N) was not significant between adult and old mice, although the data were highly variable. Data presented as mean ± standard error of the mean and analysed using two-way analyses of variance with Sidak's *post hoc* test. $^{*}P \leq 0.05$ and $^{\#}P \leq 0.1$. '$' indicates a magnitude effect between adult and old mice.

DOI: 10.1002/jcsm.12685

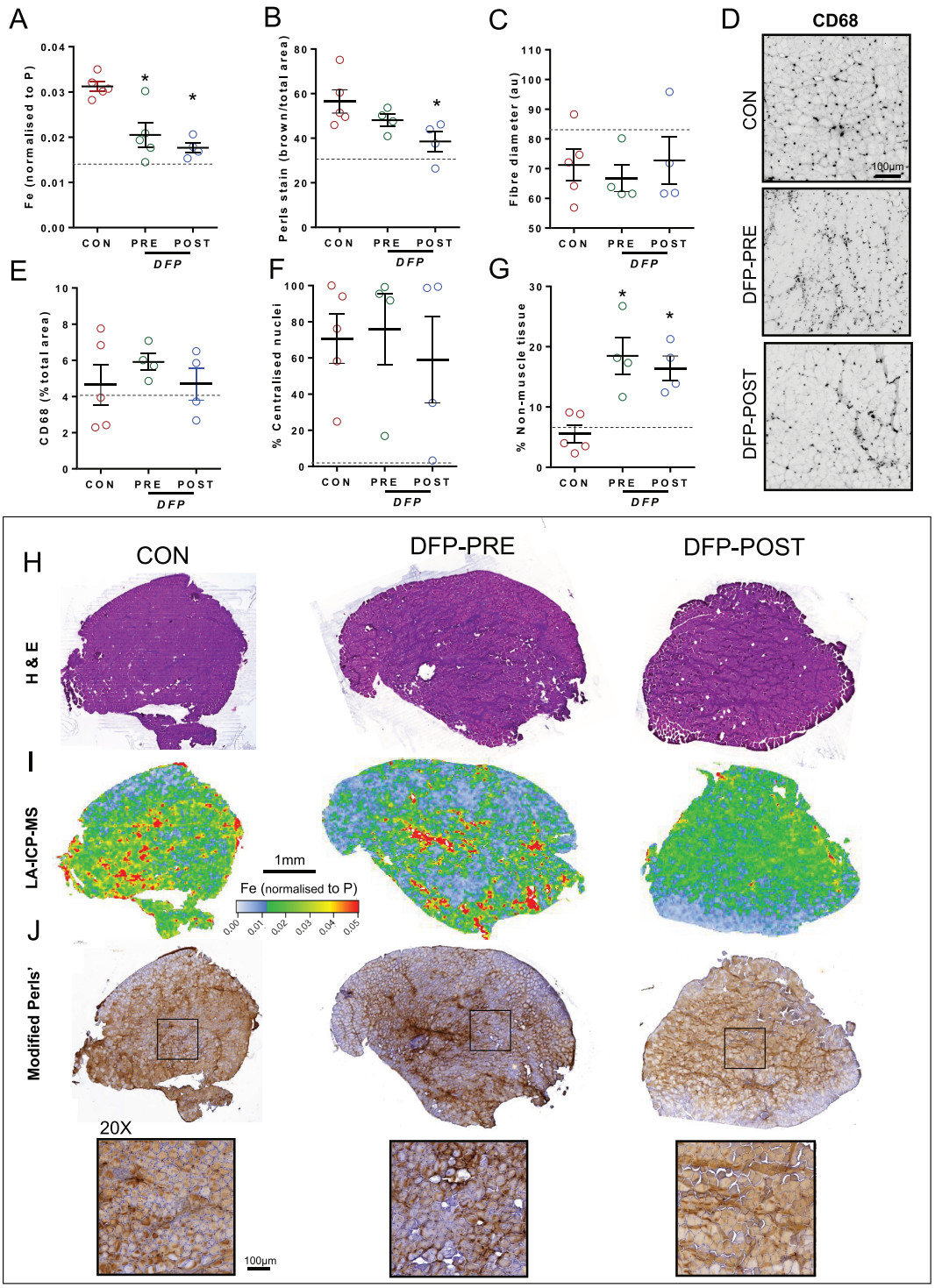

Figure 5 Control old mice (n = 6) were subject to ischaemia–reperfusion injury (IRI) prior to 14 days of recovery. DFP-PRE old mice (n = 4) were treated with DFP (150 mg/kg/day) for 7 days prior to IRI, and DFP-POST old mice (n = 5) were treated with DFP (150 mg/kg/day) for 14 days after IRI. This involved application of an orthodontic rubber band above the knee of the right leg for 90 min of ischaemia with subsequent reperfusion. Injured legs were compared between treatment groups. Both treatment approaches reduced total elemental iron (A, I) and iron, as shown in representative images of the modified Perls' stain (J) (brown = ferric Fe^{3+} deposits) and quantified (B). Fibre diameter (C), percentage of centralized myonuclei (F), and level of inflammatory cell infiltration (D, E) were unchanged. Observations of haematoxylin and eosin staining showed an increase in non-muscle tissue (adipocytes) within muscles treated with DFP (G, H). Data presented as mean ± standard error of the mean. Data were analysed using one-way analyses of variance with Tukey's (A) *post hoc* test. *$P \leq 0.05$.

DOI: 10.1002/jcsm.12685

Table 3 Correlation analyses in old mice after injury with or without deferiprone treatment

Fe vs.	*r*	*P*
NMI	−0.7837	0.01**
Fibrosis	−0.3370	0.2388
PGC-1a	0.1875	0.5208
COX IV	−0.2401	0.4083
CS	−0.2241	0.3041
CD68	−0.0132	0.9660

Injured legs from control, DFP-PRE, and DFP-POST old mice were pooled together (n = 15). Total iron (Fe measured by laser ablation inductively coupled plasma mass spectrometry) was positively correlated (Pearson's r) with non-muscle infiltration (NMI). No correlation (Pearson's r) was found in a marker of mitochondria content, protein expression of peroxisome proliferator-activated receptor gamma coactivator 1-alpha (PGC-1a), cytochrome *c* oxidase (COX IV), citrate synthase activity (CS), and immunohistochemistry of inflammatory mediator cluster of differentiation 68 (CD68). CS and COX IV were measured in the gastrocnemius muscles. All other measurements were taken from the tibialis anterior muscles.

studies have investigated links between iron, oxidative stress, lipid peroxidation, and skeletal muscle size, but the consensus is that muscle iron accumulation is associated with reduced muscle mass.[7,11–13] Here, we demonstrated that tissue iron is elevated in a murine model of sarcopenia, which was associated with increased lipid peroxidation and skeletal muscle atrophy. Treatment with a common iron chelator (DFP) did not reduce skeletal muscle iron in muscles of old mice, indicating that other therapeutic approaches are needed to address muscle iron overload and its downstream complications. The muscles of old mice with elevated iron exhibited impaired muscle regeneration after lower-limb IR damage. The injury exacerbated iron dysregulation in old mice, and rather than accelerating the repair of muscle, iron chelation with DFP administration before and after IR injury further impaired muscle regeneration. These findings provide new insights into iron changes that occur with age and injury, and the importance of this element in muscle maintenance and repair.

Increased intracellular iron and lipid peroxidation is associated with age-related muscle atrophy

Old (~24-month-old) 129SvEv FVBM mice exhibited skeletal muscle atrophy and weakness similar to that reported previously in the commonly used C57BL/6J mouse model of sarcopenia.[39,40] Old 129SvEv FVBM mice were heavier than similar old C57BL/6J mice, but key parameters of an ageing phenotype (compared with that of young adult mice) were consistent, including an increased body mass due predominantly to an increased fat mass, decreased voluntary running distance, decreased metabolic rate (normalized to body mass), proportional substrate preference towards fat, and decreased grip strength.[39,40] Like in old C57BL/6J mice, assessments of muscle cross-sections revealed that old 129SvEv FVBM mice had smaller muscle fibres and an increased number of fibres with central nuclei.[41] The similarity in attributes confirmed the suitability of the old 129SvEv FVBM mouse as a model for studying sarcopenia.

To our knowledge, these findings are the first to demonstrate iron overload in a mouse model of sarcopenia using mass spectrometry imaging (LA-ICP-MS) to visualize the distribution of total elemental iron in muscle cross-sections. Combining LA-ICP-MS with H&E staining of the same cross-sections allowed assessment of the localization of intramuscular iron. Furthermore, we assessed ferric iron using modified Perls' stain and the presence of inflammatory cells in muscle cross-sections. Based on our observations of unchanged inflammatory cell numbers within muscle sections between adult and old mice and Perls' staining revealing brown staining predominantly within fibres, we provide evidence that the iron overload occurs within muscle cells with ageing. Our observations are in accordance with reports of increased total iron and ferritin in muscles of 30-month-old male F344xBN FI rats[12] and support our hypothesis that iron overload represents a potential therapeutic target for sarcopenia.

Mitochondrial and metabolic dysfunctions are well-known phenomena in sarcopenia.[42] We found that muscles from old mice had smaller fibres and increased oxidative stress, evidenced by increased lipid peroxidation (4HNE), increased iron-containing proteins (ferritin, FTH), and changes in mitochondrial markers (including decreased ALAS-1 and CYT-C). Combined with iron overload, these observations suggest that during ageing, muscles experience oxidative stress that contributes to muscle atrophy and impaired regeneration. The correlation of increased iron and lipid peroxidation is also characteristic of a newly identified cell death pathway known as ferroptosis. Ferroptosis is phenotypically different from apoptosis, unregulated necrosis, and necroptosis[43] and has distinguishing morphological features involving increased lipid peroxidation leading to disruptions to mitochondrial membrane and dysfunction.[44] Our observations are also in line with studies where direct iron administration (via intraperitoneal injection) to healthy adult mice induced muscle atrophy due to elevated oxidative stress.[13,17,45] In addition, iron administration suppressed differentiation of C2C12 myoblasts *in vitro* and reduced myotube diameter,[13,45] implicating iron-induced oxidative stress for the impaired Akt/FOXO and MAPK signalling and increased E3 ubiquitin ligase activity.[13]

We observed more 4HNE abundance in muscles of old mice, confirming previous reports of an age-related increase in malondialdehyde content in skeletal muscle,[46] thus highlighting lipid peroxidation as a feature of sarcopenia. In myotubes, lipid peroxidation via administration of malondialdehyde impaired proliferation and differentiation of skeletal muscle myoblasts.[47] No studies have directly administered lipid peroxides to muscle to assess a direct relationship with muscle wasting, but administration of a potent

lipid peroxidation inhibitor (IRFI-042: a vitamin E-like antioxidant) increased forelimb strength and decreased fatigue in *mdx* dystrophic mice, where muscle wasting is characterized by increased lipid peroxidation.[48] IRFI-042 blunted NF-κB DNA-binding activity and tumour necrosis factor-α expression, resulting in decreased necrosis and increased muscle fibre regeneration.[48] Based on the observed dysregulation in iron homeostasis, we proposed that iron chelation could counteract sarcopenia.

Oral administration of an iron chelator (deferiprone) does not modulate iron in muscles of old mice

To counteract iron overload, we directly targeted iron via DFP. *In vitro* experiments had shown that DFP induced iron deficiency in C2C12 myotubes leading to mitochondrial impairments,[49] highlighting the need for iron in cellular respiration and the potential for DFP to manage iron overload. Surprisingly, we found that chronic (12 week) DFP treatment in old mice reduced iron in the liver but not in skeletal muscle. Although these results seemingly contradict DFP's ability to redistribute iron from skeletal muscles, the results are consistent with observations that administration of the iron chelator, pyridoxal isonicotinoyl hydrasone, did not alter non-haem iron or muscle size in 30-month-old rats.[12] Combined, these data may suggest that iron chelator treatment is not effective in modulating iron in old muscle cells that have increased ferritin expression. Interestingly, DFP treatment was also ineffective in chelating iron in senescent (due to iron overload) mouse embryonic fibroblast model.[50] Iron stored in ferritin is considered to be disabled and 'safe' from generating ROS, but it is also unable to be incorporated into key proteins required for cellular respiration as evidenced by our observation of reduced protein levels of CYT-C and ALAS-1 creating a perceived deficiency.[50] Therefore, treatments that enhance the breakdown of ferritin, which is dependent on autophagy,[51–53] may be beneficial. As autophagy is clearly disrupted in old muscles,[54] we propose that interventions that stimulate autophagy such as rapamycin treatment[55] and calorie restriction[56] could improve skeletal muscle iron homeostasis via facilitating ferritinophagy.

Elevated iron: good or bad during regeneration after injury?

Some surgeries on older patients (including joint replacements and limb revascularization) require temporary occlusion of blood flow, which induces ischaemia and compromises the muscle's local milieu. Reperfusion, while necessary to avert hypoxic muscle damage, paradoxically introduces a new oxygen chemical lesion that exacerbates local tissue injury.[57] Generally, hypoxia during ischaemia facilitates iron import into tissues (i.e. kidney) and increases ROS generation.[58] In our model of IR, iron was not elevated in damaged muscles at 4 h, 1 day, or 3 days after injury but elevated at 7 and 14 days, suggesting that hypoxia did not acutely increase muscle iron content and that other regulatory processes are involved. While iron elevation has not yet been investigated in response to muscle ischaemia and reperfusion, models of hindlimb suspension have shown increases of iron in muscles after 7 and 14 days immobilization.[10] Our time course investigation suggests that iron content coincides with regeneration rather than during the ischaemic insult.

The higher basal amount of iron in muscles with ageing provides a stimulus for ROS generation during the reperfusion after ischaemia. Indeed, muscles from old mice had altered mitochondrial enzyme activity and higher levels of iron, lipid peroxidation, and delayed regeneration and more profound deposition of fibrosis, indicating aggravated muscle damage in old mice. These observations are consistent with studies in the liver and brain, where iron overload is a risk factor for IRI, and lipid peroxidation is a cause of ferroptotic cell death.[59,60] While ferroptosis has not been explored in muscle, mice injected with iron before a cardiotoxin injury exhibit increased oxidative stress and decreased satellite cell markers associated with signs of delayed regeneration.[13] In addition, lipid peroxidation generated by microtrauma to muscle after exercise is also increased in iron supplemented adults and children.[61]

Based on these observations, we investigated whether lowering iron in skeletal muscles of old mice would affect the response to IR injury. In contrast to our long-term treatment with DFP in uninjured old mice, we demonstrated that treatment with DFP before or after IRI injury reduced iron in muscle but also impaired regeneration 14 days after injury. These observations highlight the inherent differences in the local muscle environment between injured and uninjured muscle tissues and the ability of DFP to chelate iron under these conditions. Necrosis of muscle fibres enables the release of iron from myoglobin and other haem proteins. However, the ROS generating potential of iron is mitigated by infiltrating macrophages that engulf and detoxify haem.[62] At later stages in regeneration, macrophages increase expression of ferroportin (FPN) and switch from iron scavengers to recyclers.[14] Regenerating muscle concomitantly expresses high levels of TfR1 to import iron for essential metabolic regeneration.[14] It is likely that DFP interferes with this dynamic process that only occurs during injury and regeneration, explaining the discrepancy of DFP's efficacy. These findings highlight an important role of iron in facilitating effective muscle repair. We have shown in adult BL6 mice that inflammatory cell infiltration (i.e. macrophages, Day 3 and Day 7) precede and overlap with the increase of iron (Day 7 and Day 14) after IR injury. Recent studies using macrophages from FPN KO mice demonstrated that iron recycling by macrophages is essential for muscle

regeneration. Macrophages that lack FPN were unable to redistribute iron back into muscles after injury, ultimately resulting in iron accumulation within muscle-infiltrating macrophages and impairing regeneration that promoted fat accumulation.[14] We propose that the DFP treatment before and after IRI treatments chelated the excess iron that would normally support muscle regeneration, leading to the significantly increased deposition of fat and metabolic dysfunction.

These observations suggest that alternative interventions such as drugs that inhibit the deleterious oxidative chemistry of iron (including novel lipid antioxidants such as ferrostatin-1), yet do not remove iron that is necessary for muscle growth, should be explored.

Conclusions

We have shown that muscles from old mice have increased iron levels, which are associated with increased lipid peroxidation, increased susceptibility to IR injury, and impaired muscle regeneration. Chronic treatment with an iron chelator did not redistribute iron in muscles of old mice, highlighting the complexity of restricting iron in the context of muscle ageing and regeneration. Our results suggest that iron is involved in effective muscle regeneration and highlight the importance of iron homeostasis in muscle atrophy and regeneration.

Acknowledgements

The authors of this manuscript certify that they comply with the ethical guidelines for authorship and publishing in the *Journal of Cachexia, Sarcopenia and Muscle*.[63]

Funding

This work was supported by infrastructure and technical assistance from the Melbourne Mouse Metabolic Phenotyping Platform (MMMPP) at the University of Melbourne.

Online supplementary material

Additional supporting information may be found online in the Supporting Information section at the end of the article.

Figure S1. Analysis of several inflammatory and energetic genes and proteins in old mice (22–24 months, n = 4–6) compared to adult mice (12 weeks, n = 6) there was change in energetic mRNA expression (A) Delta-aminolevulinate synthase 1, *Alas-1*; Carnitine palmitoyltransferase I, *Cpt 1*; cytochrome c oxidase, *Cox IV*; Peroxisome proliferator-activated receptor gamma coactivator 1-alpha, *Ppargc1a*; (B) protein expression of Peroxisome proliferator-activated receptor gamma coactivator 1-alpha, PGC-1a; or COX IV, and (C) Citrate Synthase activity. (D) mRNA expression of inflammatory mediators Cluster of Differentiation 68, *Cd68*; EGF-like module-containing mucin-like hormone receptor-like 1, *F4/80*; mannose receptor, *Cd206*; Scavenger receptor cysteine-rich type 1 protein; *Cd163*, T-lymphocyte activation antigen; *Cd80*, interleukin-6, Il-6; suppressor of cytokine signaling 3, *Socs3* and chemokine ligand 2, *Ccl2*. Data presented as mean ± SEM. Data were analysed using Student's t-test. *$P \leq 0.05$ and # $P \leq 0.1$ compared to Adult.

Figure S2. A time course study was conducted in 12-week-old BL6 mice. Ischemia–reperfusion injury involved application of an orthodontic rubber band above the knee for 90-minutes of ischemia and subsequent reperfusion. N = 5 mice were then culled at several timepoints after reperfusion: 4 hours, 1 day, 3 days, 7 days and 14 days. Representative images for muscle structure (haematoxylin and eosin), inflammatory cells (CD68/F480/DAPI) and fibrosis (Van Gieson's) of the tibialis anterior (TA) muscle (A). TA muscle mass (B) and inflammatory cells (C, F) varied over the time course along with iron (D), calcium (E) levels determined via IC-PMS and fibrosis (G). Data presented as mean ± SEM and analysed using two-way ANOVA with Sidek multiple comparisons test *$P \leq 0.05$ compared to injured leg.

Figure S3. Adult and old mice (n = 6/group) were subject to ischemia reperfusion injury (IRI) and 14 days of recovery. This involved application of an orthodontic rubber band above the knee to the right leg (I = injured) for a 90-minute period of ischemia and subsequent reperfusion. Injured legs were compared to contralateral left uninjured legs (C = control). Grey = Adult and Red = old. Representative images of fibrosis (Van Gieson's) (A) show increased fibrosis which associated with mRNA of collagen type I and III, *Col1a1 andCol3a1* (B) mRNA expression of inflammatory mediators Cluster of Differentiation 68, *Cd68*; EGF-like module-containing mucin-like hormone receptor-like 1, *F4/80*; mannose receptor, *Cd206*; Scavenger receptor cysteine-rich type 1 protein; *Cd163*, T-lymphocyte activation antigen; *Cd80*, interleukin-6, and *Il-6*; suppressor of cytokine signaling 3, *Socs3* were variable and showed no differences. Data presented as mean ± SEM and analysed using two-way ANOVAs with Sidak's post hoc test. *$P \leq 0.05$ and # $P \leq 0.1$

Figure S4. Control old mice (n = 4) were subject to ischemia reperfusion injury (IRI) followed by 14 days of recovery. DFP-PRE old mice (n = 4) were treated with DFP (150 mg/kg/day) for 7 days prior to IRI and DFP-POST old mice (n = 4) were treated with DFP (150 mg/kg/day) for 14 days post IRI. Injured legs were compared between treatment groups. Representative images of fibrosis (A) showed no difference between treatments (B) or mRNA of collagen type I

and III, *Col1a1* and*Col3a1* (C). Western blots of homogenised gastrocnemius muscles showed no change in the expression of (D) Peroxisome proliferator-activated receptor gamma coactivator 1-alpha, PGC-1a; or COX IV, but Citrate Synthase activity was reduced with pre treatment of DFP (E). Analysis mRNA expression of inflammatory mediators Cluster of Differentiation 68, CD68; EGF-like module-containing mucin-like hormone receptor-like 1, F4/80; mannose receptor, Cd206; Scavenger receptor cysteine-rich type 1 protein; CD163, T-lymphocyte activation antigen; CD80, interleukin-6, and Il-6; suppressor of cytokine signaling 3, Socs3 were variable and showed no differences. Data presented as mean ± SEM. Data were analysed using one-way ANOVAs with Tukey's (A) post hoc test. $*P \leq 0.05$ compared to Old injured leg.

Conflict of interest

A.I.B. is a shareholder in Alterity Ltd, Cogstate Ltd, Brighton Biotech LLC, Grunbiotics Pty Ltd, Eucalyptus Pty Ltd, and Mesoblast Ltd. He is a paid consultant for, and has a profit share interest in, Collaborative Medicinal Development Pty Ltd.

References

1. Wilkinson DJ, Piasecki M, Atherton PJ. The age-related loss of skeletal muscle mass and function: measurement and physiology of muscle fibre atrophy and muscle fibre loss in humans. *Ageing Res Rev* 2018;**47**:123–132.
2. von Haehling S, Morley JE, Anker SD. An overview of sarcopenia: facts and numbers on prevalence and clinical impact. *J Cachexia Sarcopenia Muscle* 2010;**1**:129–133.
3. Peng TC, Chen WL, Wu LW, Chang YW, Kao TW. Sarcopenia and cognitive impairment: a systematic review and meta-analysis. *Clin Nutr* 2019;**39**:2695–2701.
4. Cabett Cipolli G, Sanches Yassuda M, Aprahamian I. Sarcopenia is associated with cognitive impairment in older adults: a systematic review and meta-analysis. *J Nutr Health Aging* 2019;**23**:525–531.
5. Dhillon RJ, Hasni S. Pathogenesis and management of sarcopenia. *Clin Geriatr Med* 2017;**33**:17–26.
6. Finkel T, Holbrook NJ. Oxidants, oxidative stress and the biology of ageing. *Nature* 2000;**408**:239–247.
7. Altun M, Edström E, Spooner E, Flores-Moralez A, Bergman E, Tollet-Egnell P, et al. Iron load and redox stress in skeletal muscle of aged rats. *Muscle Nerve* 2007;**36**:223–233.
8. Hofer T, Marzetti E, Xu J, Seo AY, Gulec S, Knutson MD, et al. Increased iron content and RNA oxidative damage in skeletal muscle with aging and disuse atrophy. *Exp Gerontol* 2008;**43**:563–570.
9. Atamna H. Heme, iron, and the mitochondrial decay of ageing. *Ageing Res Rev* 2004;**3**:303–318.
10. Xu J, Hwang JC, Lees HA, Wohlgemuth SE, Knutson MD, Judge AR, et al. Long-term perturbation of muscle iron homeostasis following hindlimb suspension in old rats is associated with high levels of oxidative stress and impaired recovery from atrophy. *Exp Gerontol* 2012;**47**:100–108.
11. Jung SH, DeRuisseau LR, Kavazis AN, DeRuisseau KC. Plantaris muscle of aged rats demonstrates iron accumulation and altered expression of iron regulation proteins. *Exp Physiol* 2008;**93**:407–414.
12. DeRuisseau KC, Park YM, DeRuisseau LR, Cowley PM, Fazen CH, Doyle RP. Aging-related changes in the iron status of skeletal muscle. *Exp Gerontol* 2013;**48**:1294–1302.
13. Ikeda Y, Satoh A, Horinouchi Y, Hamano H, Watanabe H, Imao M, et al. Iron accumulation causes impaired myogenesis correlated with MAPK signaling pathway inhibition by oxidative stress. *FASEB J* 2019;**33**:9551–9564.
14. Corna G, Caserta I, Monno A, Apostoli P, Manfredi AA, Camaschella C, et al. The repair of skeletal muscle requires iron recycling through macrophage ferroportin. *J Immunol* 2016;**197**:1914–1925.
15. Barbieri E, Sestili P. Reactive oxygen species in skeletal muscle signaling. *J Signal Transduct* 2012;**2012**:982794.
16. Finch CA, Huebers H. Perspectives in iron metabolism. *N Engl J Med* 1982;**306**:1520–1528.
17. Reardon TF, Allen DG. Iron injections in mice increase skeletal muscle iron content, induce oxidative stress and reduce exercise performance. *Exp Physiol* 2009;**94**:720–730.
18. Ayton S, Lei P, Adlard PA, Volitakis I, Cherny RA, Bush AI, *et al*. Iron accumulation confers neurotoxicity to a vulnerable population of nigral neurons: implications for Parkinson's disease. *Mol Neurodegener* 2014;**9**:27.
19. Sotoudeh A, Takhtfooladi MA, Jahanshahi A, Asl AH, Takhtfooladi HA, Khansari M. Effect of N-acetylcysteine on lung injury induced by skeletal muscle ischemia-reperfusion. Histopathlogical study in rat model. *Acta Cir Bras* 2012;**27**:168–171.
20. Takhtfooladi MA, Jahanshahi A, Jahanshahi G, Sotoudeh A, Takhtfooladi HA, Khansari M. Protective effect of N-acetylcysteine on kidney as a remote organ after skeletal muscle ischemia-reperfusion. *Acta Cir Bras* 2012;**27**:611–615.
21. Beyersdorf F, Unger A, Wildhirt A, Kretzer U, Deutschländer N, Krüger S, et al. Studies of reperfusion injury in skeletal muscle: preserved cellular viability after extended periods of warm ischemia. *J Cardiovasc Surg (Torino)* 1991;**32**:664–676.
22. Crawford RS, Hashmi FF, Jones JE, Albadawi H, McCormack M, Eberlin K, *et al*. A novel model of acute murine hindlimb ischemia. *Am J Physiol Heart Circ Physiol* 2007;**292** (2):H830–837.
23. Ham DJ, Gardner A, Kennedy TL, Trieu J, Naim T, Chee A, et al. Glycine administration attenuates progression of dystrophic pathology in prednisolone-treated dystrophin/utrophin null mice. *Sci Rep* 2019;**9**:12982.
24. Haynes VR, Keenan SN, Bayliss J, Lloyd EM, Meikle PJ, Grounds MD, et al. Dysferlin deficiency alters lipid metabolism and remodels the skeletal muscle lipidome in mice. *J Lipid Res* 2019;**60**:1350–1364.
25. Schertzer JD, Gehrig SM, Ryall JG, Lynch GS. Modulation of insulin-like growth factor (IGF)-I and IGF-binding protein interactions enhances skeletal muscle regeneration and ameliorates the dystrophic pathology in *mdx* mice. *Am J Pathol* 2007;**171**:1180–1188.
26. Gehrig SM, Ryall JG, Schertzer JD, Lynch GS. Insulin-like growth factor-I analogue protects muscles of dystrophic *mdx* mice from contraction-mediated damage. *Exp Physiol* 2008;**93**:1190–1198.
27. Caldow MK, Ham DJ, Chee A, Trieu J, Naim T, Stapleton DI, et al. Muscle-specific deletion of SOCS3 does not reduce the anabolic response to leucine in a mouse model of acute inflammation. *Cytokine* 2017;**96**:274–278.
28. Ham DJ, Caldow MK, Chhen V, Chee A, Wang X, Proud CG, et al. Glycine restores the anabolic response to leucine in a

mouse model of acute inflammation. *Am J Physiol Endocrinol Metab* 2016;**310**: E970–E981.
29. Swiderski K, Todorov M, Gehrig SM, Naim T, Chee A, Stapleton DI, et al. Tranilast administration reduces fibrosis and improves fatigue resistance in muscles of *mdx* dystrophic mice. *Fibrogenesis Tissue Repair* 2014;**7**:1.
30. Gehrig SM, van der Poel C, Sayer TA, Schertzer JD, Henstridge DC, Church JE, et al. Hsp72 preserves muscle function and slows progression of severe muscular dystrophy. *Nature* 2012;**484**:394–398.
31. Swiderski K, Thakur SS, Naim T, Trieu J, Chee A, Stapleton DI, et al. Muscle-specific deletion of SOCS3 increases the early inflammatory response but does not affect regeneration after myotoxic injury. *Skelet Muscle* 2016;**6**:36.
32. Smith MA, Harris PL, Sayre LM, Perry G. Iron accumulation in Alzheimer disease is a source of redox-generated free radicals. *Proc Natl Acad Sci USA* 1997;**94**: 9866–9868.
33. Schindelin J, Arganda-Carreras I, Frise E, Kaynig V, Longair M, Pietzsch T, et al. Fiji: an open-source platform for biological-image analysis. *Nat Methods* 2012;**9**:676–682.
34. James SA, Churches QI, de Jonge MD, Birchall IE, Streltsov V, McColl G, et al. Iron, copper, and zinc concentration in Aβ plaques in the APP/PS1 mouse model of Alzheimer's disease correlates with metal levels in the surrounding neuropil. *ACS Chem Neurosci* 2017;**8**:629–637.
35. Hare DJ, Fryer F, Paul B, Bishop DP, Doble PA. Characterisation of matrix-based polyatomic interference formation in laser ablation-inductively coupled plasma-mass spectrometry using dried micro-droplet ablation and its relevance for bioimaging. *Anal Methods* 2016;**8**:7552–7556.
36. Kysenius K, Paul B, Hilton JB, Liddell JR, Hare DJ, Crouch PJ. A versatile quantitative microdroplet elemental imaging method optimised for integration in biochemical workflows for low-volume samples. *Anal Bioanal Chem* 2019;**411**: 603–616.
37. Bishop DP, Clases D, Fryer F, Williams E, Wilkins S, Hare DJ, et al. Elemental bio-imaging using laser ablation-triple quadrupole-ICP-MS. *J Anal At Spectrom* 2016;**31**:197–202.
38. Grehn M, Seuthe T, Höfner M, Griga N, Theiss C, Mermillod-Blondin A, et al. Femtosecond-laser induced ablation of silicate glasses and the intrinsic dissociation energy. *Opt Mater Express* 2014;**4**: 689–700.
39. Houtkooper RH, Argmann C, Houten SM, Cantó C, Jeninga EH, Andreux PA, et al. The metabolic footprint of aging in mice. *Sci Rep* 2011;**1**:134.
40. Takeshita H, Yamamoto K, Nozato S, Inagaki T, Tsuchimochi H, Shirai M, et al. Modified forelimb grip strength test detects aging-associated physiological decline in skeletal muscle function in male mice. *Sci Rep* 2017;**7**:42323.
41. Lin IH, Chang JL, Hua K, Huang WC, Hsu MT, Chen YF. Skeletal muscle in aged mice reveals extensive transformation of muscle gene expression. *BMC Genet* 2018;**19**:55.
42. Coen PM, Musci RV, Hinkley JM, Miller BF. Mitochondria as a target for mitigating sarcopenia. *Front Physiol* 2018;**9**:1883.
43. Yang WS, Stockwell BR. Ferroptosis: death by lipid peroxidation. *Trends Cell Biol* 2016;**26**:165–176.
44. Stockwell BR, Angeli JP, Bayir H, Bush AI, Conrad M, Dixon SJ, et al. Ferroptosis: a regulated cell death nexus linking metabolism, redox biology, and disease. *Cell* 2017;**171**:273–285.
45. Ikeda Y, Imao M, Satoh A, Watanabe H, Hamano H, Horinouchi Y, et al. Iron-induced skeletal muscle atrophy involves an Akt-forkhead box O3–E3 ubiquitin ligase-dependent pathway. *J Trace Elem Med Biol* 2016;**35**:66–76.
46. Marzani B, Felzani G, Bellomo RG, Vecchiet J, Marzatico F. Human muscle aging: ROS-mediated alterations in rectus abdominis and vastus lateralis muscles. *Exp Gerontol* 2005;**40**:959–965.
47. Dodgen AK-E, Shanmugam G, Namakkal-Soorappan R. 53—Lipid peroxidation impairs proliferation and differentiation of skeletal muscle myoblasts in vitro. *Free Radic Biol Med* 2017;**112**:50–51.
48. Messina S, Altavilla D, Aguennouz MH, Seminara P, Minutoli L, Monici MC, et al. Lipid peroxidation inhibition blunts nuclear factor-κB activation, reduces skeletal muscle degeneration, and enhances muscle function in *mdx* mice. *Am J Pathol* 2006;**168**:918–926.
49. Leermakers PA, Remels AH, Zonneveld MI, Rouschop KM, Schols AM, Gosker HR. Iron deficiency-induced loss of skeletal muscle mitochondrial proteins and respiratory capacity; the role of mitophagy and secretion of mitochondria-containing vesicles. *FASEB J* 2020;**34**:6703–6717.
50. Masaldan S, Clatworthy SA, Gamell C, Meggyesy PM, Rigopoulos AT, Haupt S, et al. Iron accumulation in senescent cells is coupled with impaired ferritinophagy and inhibition of ferroptosis. *Redox Biol* 2018;**14**:100–115.
51. Radisky DC, Kaplan J. Iron in cytosolic ferritin can be recycled through lysosomal degradation in human fibroblasts. *Biochem J* 1998;**336**:201–205.
52. Mancias JD, Kimmelman AC. Mechanisms of selective autophagy in normal physiology and cancer. *J Mol Biol* 2016;**428**:1659–1680.
53. Asano T, Komatsu M, Yamaguchi-Iwai Y, Ishikawa F, Mizushima N, Iwai K. Distinct mechanisms of ferritin delivery to lysosomes in iron-depleted and iron-replete cells. *Mol Cell Biol* 2011;**31**:2040–2052.
54. Carnio S, LoVerso F, Baraibar MA, Longa E, Khan MM, Maffei M, et al. Autophagy impairment in muscle induces neuromuscular junction degeneration and precocious aging. *Cell Rep* 2014;**8**:1509–1521.
55. Kawakami Y, Hambright WS, Takayama K, Mu X, Lu A, Cummins JH, et al. Rapamycin rescues age-related changes in muscle-derived stem/progenitor cells from progeroid mice. *Mol Ther Methods Clin Dev* 2019;**14**:64–76.
56. Chung KW, Chung HY. The effects of calorie restriction on autophagy: role on aging intervention. *Nutrients* 2019;**11**:2923.
57. Yassin MM, Harkin DW, D'Sa AA, Halliday MI, Rowlands BJ. Lower limb ischemia-reperfusion injury triggers a systemic inflammatory response and multiple organ dysfunction. *World J Surg* 2002;**26**:115–121.
58. van Swelm RPL, Wetzels JFM, Swinkels DW. The multifaceted role of iron in renal health and disease. *Nat Rev Nephrol* 2020;**16**:77–98.
59. Yamada N, Karasawa T, Wakiya T, Sadatomo A, Ito H, Kamata R, et al. Iron overload as a risk factor for hepatic ischemia-reperfusion injury in liver transplantation: potential role of ferroptosis. *Am J Transplant* 2020;**20**:1606–1618.
60. Wan J, Ren H, Wang J. Iron toxicity, lipid peroxidation and ferroptosis after intracerebral haemorrhage. *Stroke Vasc Neurol* 2019;**4**:93–95.
61. Deli CK, Fatouros IG, Paschalis V, Tsiokanos A, Georgakouli K, Zalavras A, et al. Iron supplementation effects on redox status following aseptic skeletal muscle trauma in adults and children. *Oxid Med Cell Longev* 2017;**2017**:4120421.
62. Hentze MW, Muckenthaler MU, Galy B, Camaschella C. Two to tango: regulation of mammalian iron metabolism. *Cell* 2010;**142**:24–38.
63. von Haehling S, Morley JE, Coats AJ, Anker SD. Ethical guidelines for publishing in the Journal of Cachexia, Sarcopenia and Muscle: update 2019. *J Cachexia Sarcopenia Muscle* 2019;**10**:1143–1145.